Journal of Neural Engineering

OPEN ACCESS

RECEIVED
21 February 2023

REVISED
27 May 2024

ACCEPTED FOR PUBLICATION
6 June 2024

PUBLISHED
19 June 2024

PAPER

Deep brain stimulation pulse sequences to optimally modulate frequency-specific neural activity

Hafsa Farooqi[1], **Jerrold L Vitek**[1] **and David Escobar Sanabria**[2,*]

[1] Department of Neurology, Medical School, University of Minnesota, Minneapolis, MN 55455, United States of America
[2] Department of Biomedical Engineering, Lerner Research Institute, Cleveland Clinic, Cleveland, OH 44195, United States of America
* Author to whom any correspondence should be addressed.

E-mail: escobad2@ccf.org

Keywords: deep brain stimulation, optimization, neuromodulation, Parkinson's disease, stimulation-evoked neural responses, mathematical models

Abstract

Objective. Precise neuromodulation systems are needed to identify the role of neural oscillatory dynamics in brain function and to advance the development of brain stimulation therapies tailored to each patient's signature of brain dysfunction. Low-frequency, local field potentials (LFPs) are of increasing interest for the development of these systems because they can reflect the synaptic inputs to a recorded neuronal population and can be chronically recorded in humans. In this computational study, we aim to identify stimulation pulse patterns needed to optimally maximize the suppression or amplification of frequency-specific neural activity. *Approach*. We derived DBS pulse patterns to minimize or maximize the 2-norm of frequency-specific neural oscillations using a generalized mathematical model of spontaneous and stimulation-evoked LFP activity, and a subject-specific model of neural dynamics in the pallidum of a Parkinson's disease patient. We leveraged convex and mixed-integer optimization tools to identify these pulse patterns, and employed constraints on the pulse frequency and amplitude that are required to keep electrical stimulation within its safety envelope. *Main results*. Our analysis revealed that a combination of phase, amplitude, and frequency pulse modulation is needed to attain optimal suppression or amplification of the targeted oscillations. Phase modulation is sufficient to modulate oscillations with a constant amplitude envelope. To attain optimal modulation for oscillations with a time-varying envelope, a trade-off between frequency and amplitude pulse modulation is needed. The optimized pulse sequences were invariant to changes in the dynamics of stimulation-evoked neural activity, including changes in damping and natural frequency or complexity (i.e. generalized vs. patient-specific model). *Significance*. Our results provide insight into the structure of pulse patterns for future closed-loop brain stimulation strategies aimed at controlling neural activity precisely and in real-time.

1. Introduction

Robust and precise neural control methodologies are needed to characterize the role of neural activity in the manifestation of brain conditions, and to advance the development of neuromodulation technologies. Of particular interest for the development of these technologies are the local field potentials (LFPs) recorded chronically in humans using macro-electrodes given the stability of these LFPs over time [1, 2]. Experimental and theoretical studies have shown that LFP neural activity at low-frequency (<100 Hz) is dominated by synchronized synaptic inputs to neuronal populations near the recording site [3, 4]. Therefore, these LFPs can be used as a feedback signal in closed-loop systems to control synchronized synaptic activity in a neuronal population and thereby modulate information flowing into and out of the targeted neurons.

In Parkinson's disease, synchronized 11–35 Hz ('beta' band) LFP oscillations in the subthalamic nucleus (STN) or internal segment of the globus pallidus

(GPi) are hypothesized to be associated with motor dysfunction [5–10]. Deep brain stimulation (DBS) of the STN or GPi, a surgical treatment for Parkinson's disease that yields therapeutic benefit via continuous delivery of high-frequency (HF) (130 Hz) electrical pulses, can suppress the beta band oscillations. However, the mechanisms by which HF stimulation produces these physiological or therapeutic effects are not well understood [11]. Because HF DBS is proven to improve motor function (dependent variable), we cannot deductively infer whether HF stimulation-induced suppression of beta oscillations (independent variable) precedes, succeeds, or is simply unrelated (epiphenomenal) to the improvements in motor function. Clarifying whether the relationship of beta band oscillations with PD motor signs is causal or epiphenomenon is a critical step to better understand PD pathophysiology and advance personalized DBS technology in PD and other conditions. To clarify the role of frequency-specific neural oscillations, we need tools to predictably control them without introducing confounding factors (e.g. high-frequency pulses). A recent study with the 1-methyl-4-phenyl-1,2,3,6-tetrahydropyridine nonhuman primate model of Parkinson's disease showed that amplification or suppression of beta band oscillations in the STN could be achieved using STN neural responses evoked by electrical stimulation in the internal segment of the GPi [12]. The rationale behind this approach, referred to as closed-loop evoked interference deep brain stimulation (eiDBS), is that synaptic-related neural responses evoked by electrical pulses can modulate spontaneous, synaptic-related oscillations via synaptic summation when the pulses are delivered with adequate amplitude and precise timing (phase) relative to the targeted oscillation's phase [12]. Another study with rodent models of PD also supports the idea that stimulation at precise phases of the STN oscillations can be used to suppress or amplify beta oscillations in the cortex [13]. More recently, the feasibility of using eiDBS to suppress or amplify neural activity (16–22 Hz) in the human GPi using a single DBS electrode array was demonstrated in a patient (human) with Parkinson's disease [14]. While the effectiveness of eiDBS at restoring function in Parkinson's disease or other brain conditions remains to be determined, its utility in characterizing how controlled suppression or amplification of neural oscillations relates to brain function or disease is compelling. The current implementation of eiDBS delivers electrical pulses of fixed amplitude locked to the phase of frequency-specific oscillations (i.e. phase-locked stimulation). This approach can be effective in suppressing or amplifying the mean amplitude of targeted neural activity, but it is sub-optimal to suppress neural oscillations because it does not account for dynamic changes in the amplitude of spontaneous neural oscillations. Because the stimulation pulse amplitude is set constant, variations in the oscillation amplitude can result in unwanted amplification when the spontaneous oscillations are small relative to the stimulation-evoked oscillations, or sub-optimal suppression when the spontaneous oscillations are large relative to the stimulation-evoked oscillations. Identifying electrical stimulation strategies to optimally modulate neural activity is needed to address the shortcomings of the present eiDBS implementation, perform more controlled experiments to understand the causal role of brain oscillations, and advance the development of precise, patient-specific neuromodulation devices.

In this study, we identified pulse modulation patterns that optimally suppress or amplify the 2-norm of spontaneous neural activity. To discover these pulse patterns, we employed optimization tools together with generalized mathematical models that describe the temporal dynamics of spontaneous and stimulation-evoked neural activity. We considered evoked response dynamics with distinct damping coefficients and natural frequencies to understand whether the structure of the optimal pulse patterns remained invariant with changes in these dynamics. We also derived optimal stimulation sequences using a mathematical model of the evoked and spontaneous neural activity in the GPi of a Parkinson's disease patient to confirm that the structure of these pulse sequences is preserved in neural dynamics more complex than those described by the generalized mathematical model. Our methodology enabled us to consider constraints on the pulse amplitudes and frequencies to comply with devices currently cleared or approved by the U.S. Food and Drug Administration (FDA). Of note, our study focuses on identifying the optimal value of the DBS pulse amplitude at each sampling time and, thereby, the sequence of pulse amplitudes that form the overall pulse pattern. Therefore, our study is not aimed at finding optimal values of constant hyperparameters such as the stimulation frequency, pulse width, and amplitude. Additionally, this study aims to reveal the optimized pulse sequences given complete knowledge of the spontaneous neural activity time series, not a closed-loop control law for causal implementation onto a DBS device.

Our results indicate that a trade-off between phase, frequency, and amplitude pulse modulation is needed to optimally minimize or maximize the 2-norm of targeted neural activity. The pulse modulation patterns identified in this study provide the rationale to develop future closed-loop brain stimulation strategies aimed at controlling neural activity in real-time with minimum error. Optimizing these systems could, in turn, enable us to characterize the role of oscillatory dynamics in brain function and advance the development of precise, personalized neuromodulation technology.

2. Methods

2.1. Mathematical models of neural dynamics

We employed mathematical models of spontaneous and stimulation-evoked neural dynamics to identify pulse sequences that minimize the 2-norm of frequency-specific neural activity. The 2-norm of a signal is equal to its energy, which is the integral of its instantaneous power with respect to time. Therefore, by minimizing the 2-norm of a frequency-specific signal, we are minimizing its overall energy. The average power, typically used in neuroscience to measure the size of neural signals, is not used in this study because it is not a norm or used in established optimization methods. We considered a generalized mathematical model in which relevant parameters of the stimulation-evoked responses (i.e. damping and natural/resonant frequency) were varied in order to understand whether the identified pulses patterns can be applied to distinct neural dynamics. To understand whether our results with the generalized model could be used to modulate more complex, neural dynamics similar to those observed *in-vivo*, we identified optimal pulse sequences for a mathematical model of spontaneous and stimulation-evoked activity in the GPi derived with data recorded from a PD patient [14]. We considered electrical stimulation waveforms that consist of a negative followed by a positive square pulse. These two square pulses have the same amplitude and a constant pulse width (i.e. symmetric, biphasic waveform). The pulse width is equal to the sampling period used in the discretization of the evoked response mathematical model.

The effect of stimulation pulses on the neural evoked response temporal dynamics was characterized using a saturation nonlinearity (static) connected to a system of linear equations of differences (discrete time approximation of differential equations) as depicted in figure 1. This generalized model structure has been shown to approximate the linear response of neural circuitry to electrical stimulation pulses [12, 14]. The saturation nonlinearity takes a biphasic pulse and converts it into a monophasic cathodal pulse (negative phase), which dominates the neural response according to experimental data [12]. Therefore, an alternative neural dynamics model can replace the saturation nonlinearity with pulses that are strictly monophasic. Of note, the generalized model can be interpreted as a linear approximation (around equilibrium) of a mean-field neural model, typically used in neuroscience to study neuronal populations computationally or characterize neural circuits based on data [15]. The evoked response model is described by the following equations of differences

$$y_e[k] = C\vec{z}[k] + Du[k] \tag{1}$$

$$\vec{z}[k+1] = A\vec{z}[k] + Bu[k] \tag{2}$$

where $k = 0, 1, \ldots, n-1$ is the discrete time sample associated with time kt_s; t_s is the sampling time; $\vec{z}$ is the state vector; $u[k] < 0$ is the saturated, monophasic input stimulus; $y_e[k]$ is the evoked response at sample k; and A, B, C and D are constant matrices that parameterize the equations of differences. In our model, $D = 0$ since there is no feed-through gain from the stimulus to the neural response. The saturated, monophasic stimulation input is given by $u[k] = \text{sat}(\hat{u}[k] - \underline{u})$, where $\underline{u} < 0$ is an offset representing the minimum size stimulation that evokes a neural response, $\hat{u}$ is the biphasic pulse, and $\text{sat}(*)$ is the saturation operator that converts any positive value to zero. This operator is given by:

$$\text{sat}(p) = \begin{cases} p, & \text{if } p < 0 \\ 0, & \text{otherwise.} \end{cases}$$

The LFP measurement, which reflects the combined spontaneous and stimulation-evoked neural activity, is modeled as

$$y[k] = y_e[k] + b[k], \tag{3}$$

where $b[k]$ is the value of the spontaneous neural oscillations at sample k. This linear model is a low-order simplification of the interaction between the spontaneous and stimulation-evoked neural activity that has been shown to be an approximation of experimental data [12, 14]. However, of note, this LFP model does not consider saturation effects associated with the finite number of neurons in the neuronal population being modeled, high-order nonlinear dynamics, or synaptic plasticity. The spontaneous oscillations ($b[k]$) were modeled using sinusoidal functions or synthetic LFP signals that match the power spectral density (PSD) of LFPs recorded from a PD patient.

2.1.1. Generalized, low-order model

We used a second-order model of the evoked response to characterize optimal stimulation sequences that suppress or amplify spontaneous oscillations. The second-order model is given by equations (1) and (2). The following matrices describe the parameters of these equations [16]:

$$A = \begin{bmatrix} 1 & t_s \\ -t_s\omega_n^2 & -2t_s\zeta\omega_n + 1 \end{bmatrix}, \tag{4}$$

$$B = \begin{bmatrix} 0 \\ t_s k_u \omega_n^2 \end{bmatrix}, \tag{5}$$

$$C = \begin{bmatrix} 1 & 0 \end{bmatrix}, \tag{6}$$

$$D = 0, \tag{7}$$

where $\omega_n = 2\pi f_n$ is the natural angular frequency (rad/sec) of the evoked response, ζ is the damping ratio, k_u is a scalar gain, and t_s (sec) is the sampling period.

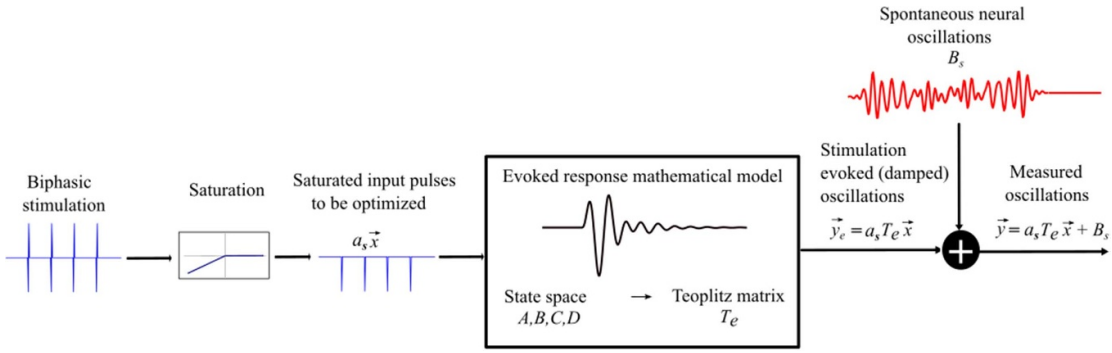

Figure 1. A schematic of the model dynamics capturing the interaction between spontaneous and stimulation-evoked neural activity in the targeted brain region. A biphasic stimulation pulse train, where each pulse is represented by a negative followed by a positive pulse, which after saturation is reduced to just the negative square pulse train. The saturated pulse train is responsible for evoking stimulation based oscillations, the dynamics of which can be mapped to a Toeplitz matrix (T_e). The final model is the summation of the matrix multiplication of the T_e with the optimization variable vector ($\vec{x}$) and the vector containing the spontaneous oscillations (B_s).

It's important to mention that any high-order mathematical model characterized by linear differential equations can be decomposed into multiple first and second-order models [17]. The second-order models, as the one described above, provide a description of the oscillatory modes in the dynamics being studied. Therefore, our analysis of a second-order system provides insights into the DBS sequences that need to be delivered to control neural dynamics driving oscillatory behavior. We considered two distinct signals to characterize the spontaneous oscillations ($b[k]$) in the generalized neural dynamics model. The first signal type is given by a sinusoidal function of frequency f_0:

$$b[k] = a_b \sin(2\pi f_0 k t_s),$$

where a_b is a constant that defines the signal amplitude. The second signal type is a sinusoidal function of frequency f_0 whose amplitude envelope is modulated by a sinusoidal of lower frequency (f_l). The following equation describes this signal:

$$b[k] = a_b \cdot (1 + \cos(2\pi f_l k t_s)) \cdot \sin(2\pi f_0 k t_s).$$

The nominal values of f_n and ζ were set equal to 20 Hz and 0.092, respectively. These parameters correspond to the frequency and damping of the dominant mode in the patient evoked response model described below. Parameters a_b, f_0, and f_l were equal to 10 μV, 20 Hz and 2 Hz, respectively. The temporal and time–frequency response to stimulation of the neural circuit's synthetic model with the above nominal parameters are depicted in figures 2(a) and (c). To understand whether the stimulation pulse sequences derived with the nominal evoked response model differed from those obtained with distinct evoked response dynamics, we characterized how deviations in ζ and f_n impact the optimized stimulation sequences. Parameters ζ and f_n were varied from 0.1 to 1, and from 10 to 30 Hz, respectively. The range

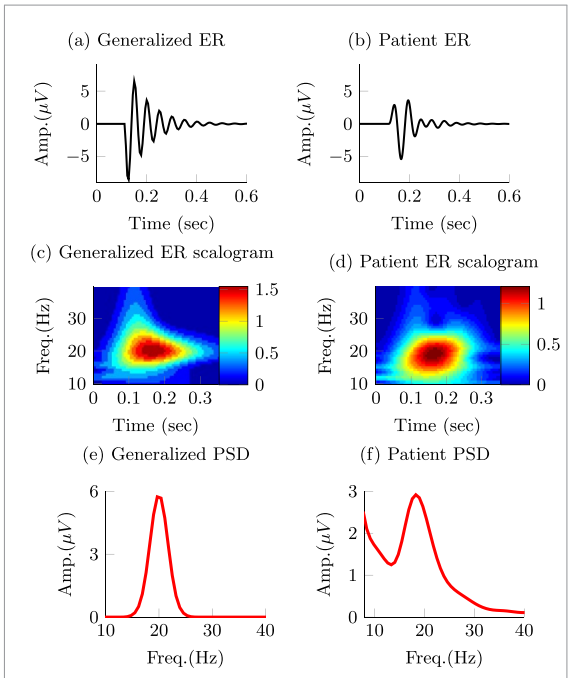

Figure 2. Stimulation-evoked responses (ER) for the generalized and patient-specific models are presented in (a) and (b), respectively. The patient-specific model characterizes the neural response in the GPi evoked by stimulation in the GPi in a PD patient. Wavelet scalograms (time–frequency maps) of the stimulation-evoked responses for the generalized mathematical model and patient-specific model are presented in (c) and (d). Power spectral density (PSD) of spontaneous LFP activity for the generalized and patient-specific models are presented in (e) and (f).

used for the damping ratio spans the neural evoked dynamics from a lightly to a highly damped response We selected a natural frequency range that deviates +/− 50% from the spontaneous oscillations' natural frequency ($f_0 = 20$ Hz).

2.1.2. Patient-specific model

A model of both spontaneous and stimulation-evoked neural activity in the GPi of a Parkinson's

disease patient was used to assess whether the results obtained with the generalized, low-order model can be applied to more complex and realistic neural dynamics. The patient-specific model was presented in a previous publication in which the input-output relationship between stimulation in the GPi and evoked responses in the GPi was estimated using instrumental variable system identification [14]. Briefly, the equations of differences describing the patient's evoked response have two imaginary pairs of poles (modes) with natural frequencies equal to 14 and 20 Hz, and corresponding damping ratios equal to 0.22 and 0.092. The frequency response of the evoked response mathematical model indicated that the largest gain in the transfer function from stimulation input to evoked response is at 19.2 Hz, near the mode with the lowest damping ($f_0 = 20$ Hz, $\zeta = 0.092$). It is worth mentioning that the transfer function gain does not peak where the dominant oscillatory mode is located (i.e. 20 Hz) because the 14 Hz mode is present, too. The time–frequency response of the neural dynamics evoked by stimulation are shown in figures 2(b)–(d) and a more detailed description of the model is presented in [14]. Having evoked response dynamics with their largest gain at 19.2 Hz implies that periodic stimuli at 19.2 Hz result in the largest steady state, periodic evoked responses at this frequency. Therefore, stimulation pulses can be used to modulate neural activity near 19.2 Hz with minimum amplitude.

The spontaneous neural activity used in the patient model was characterized by synthetic LFP signals that match the PSD observed in the GPi of a Parkinson's disease patient in the resting, awake state. The patient's evoked response model and PSD can be found in [14]. In this model, the spontaneous oscillations' frequency matches the resonant frequency of the stimulation-evoked responses. The synthetic LFP signal is given by

$$q[k] = k_\beta h_\beta[k] * n_w[k] + k_\mathrm{p} n_\mathrm{p}[k], \qquad (8)$$

where $*$ is the convolution operator, h_β is a first-order Butterworth filter with a pass-band in the 17–21 Hz range, n_w is zero mean Gaussian white noise with unitary power, n_p is a pink noise signal with unitary power, and $k_\beta = 12.6$ and $k_\mathrm{p} = 6$ are constant scalars that are adjusted to match the PSD of the studied patient. The convolution between filter h_β and the white noise n_w is equal to the modeled beta band oscillations. The filter's pass-band is centered at around 19 HZ, matching closely the frequency where the stimulation-evoked response model has its largest gain (19.2 Hz). The pink noise n_p is used to characterize the $1/f$ background activity observed in LFP neural recordings [3, 4].

The signal targeted for modulation ($b[k]$) was obtained by filtering the synthetic LFP ($q[k]$) in the 14–24 Hz band using a second order Butterworth filter. See the PSD of the synthetic LFP in figure 2(f).

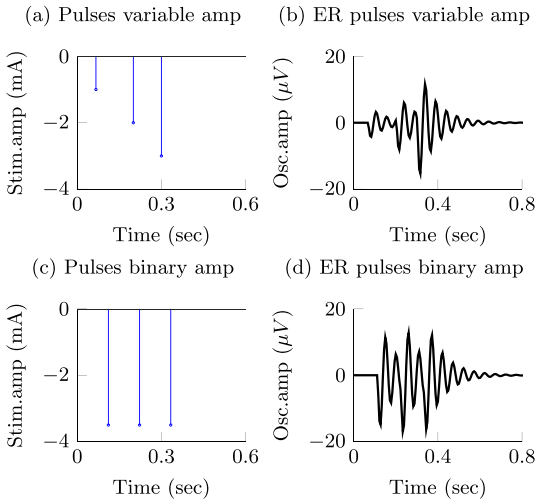

Figure 3. Examples of two different stimulation pulse patterns considered in this study and the corresponding evoked responses (ER) computed with the generalized, low-order model. A sequence of three pulses with adjustable amplitude and corresponding evoked response are presented in (a) and (b), respectively. A sequence of pulses with binary amplitude values and corresponding evoked responses are shown in (c) and (d).

2.2. Stimulation constraints

We considered stimulation sequences subject to two distinct sets of constraints in our analysis and optimization algorithms. These stimulation constraints are described below.

(i) Stimulation pulses with adjustable amplitude: this class of stimulation sequences consists of pulses whose amplitude and timing are freely selected by the optimization. An example of a stimulation sequence with varying timing and amplitude is shown in figure 3(a) and its corresponding evoked response is shown in figure 3(b). For the mathematical formulation of our optimization problem, we employed the instantaneous normalized stimulation input $x[k] = \frac{1}{a_\mathrm{s}} u[k]$ as the free optimization variable. This variable can take any value in the continuous compact interval $[-1, 0]$. a_s is a constant equal to the maximum allowed stimulation current. The input $x[k] = -1$ corresponds to stimulation pulse with the largest allowed amplitude and $x[k] = 0$ corresponds to the stimulation current that does not evoke a neural response. The values of the stimulation variable are negative or zero because the negative phase of the stimulation pulse (cathodal stimulation) was assumed to evoke the neural response [12].

(ii) Stimulation pulses with binary amplitude values: the second class of stimulation sequences consists of pulses whose amplitude can be equal to

either zero or a non-zero constant. This constraint on the stimulation pulse amplitude was studied only because present closed-loop neurostimulation systems allow us to deliver these sequences in humans [14], but not pulses whose amplitude can be adjusted in real-time. An example of a stimulation sequence with binary pulse amplitudes is shown in figure 3(c) and its corresponding evoked response is shown in figure 3(d). We used the instantaneous normalized stimulation input $x[k] = \frac{1}{a_s}u[k]$ as the optimization variable. $x[k]$ can take a value equal to either minus one or zero. Hence, a_s is the stimulation pulse amplitude when $x[k] = -1$.

2.3. Optimization approach

The goal of the optimization is to discover stimulation pulse sequences that maximize suppression or amplification of frequency-specific neural activity given the constraints described above. The mathematical function we aim to minimize is the 2-norm of the difference between the spontaneous neural activity and a reference signal to be tracked. This cost function is given by

$$J = \|\vec{y} - \vec{y}_{\text{ref}}\|_2 = \left(\sum_{k=0}^{n-1} (y[k] - y_{\text{ref}}[k])^2\right)^{1/2}, \quad (9)$$

where $\|\cdot\|_2$ represents the 2-norm and $\vec{y}_{\text{ref}}$ is the reference signal. The cost function J has the same unit as the LFP signal amplitude, which in our case is microvolts (μV). The reference signal is set equal to zero when we want to suppress the spontaneous oscillations (i.e. $\vec{y}_{\text{ref}}[k] = 0$ for all k). When we want to amplify the targeted neural activity, we set the reference signal equal to a sinusoidal with the same frequency and phase as the spontaneous oscillations but with a larger amplitude.

We considered electrical stimulation sequences with pulses delivered at samples k (i.e. samples at times kt_s). A sampling period $t_s = 1/180$ sec was used in the optimization routines to ensure that stimulation pulses were generated with a frequency smaller than or equal to the sampling frequency ($f_s = 180$ Hz). This frequency is smaller than the maximum frequency allowed in commercial DBS systems approved by the FDA for the treatment of neurological conditions [18]. This sampling frequency is also large enough to capture the neural dynamics associated with spontaneous and stimulation-evoked oscillations with a frequency below 30 Hz. To formulate the optimization problem using convex or mixed-integer tools, we represent the solution to the equations of differences (1) and (2) using a matrix multiplication:

$$\vec{y}_e = a_s T_e \vec{x}. \quad (10)$$

Vector $\vec{y}_e \in \mathbb{R}^{2n-1}$ represents the evoked response samples, vector $\vec{x} = \{x(0), \ldots, x(n-1)\} \in \mathbb{R}^n$ is the optimization pulse pattern that represents the normalized amplitude of the stimulation pulses, and T_e is a $\mathbb{R}^{(2n-1)\times n}$ Toeplitz matrix that maps the stimulation sequences to the evoked response vector [19]. The above matrix multiplication performs the convolution between the stimulation pulse pattern and the evoked response mathematical model to obtain the evoked response time series. The combined stimulation-evoked and spontaneous neural activity represented in vector form ($\vec{y} = \{y[0], \ldots, y[n-1], 0, 0, \ldots, 0\} \in \mathbb{R}^{2n-1}$) is given by

$$\vec{y} = a_s T_e \vec{x} + B_s. \quad (11)$$

Vector $B_s = \{b[0], \ldots, b[n-1], 0, 0, \ldots, 0\} \in \mathbb{R}^{2n-1}$ represents the zero-padded spontaneous neural activity. This vector is padded with zeros to match the dimensions of the Toeplitz matrix T_e, which is $\mathbb{R}^{(2n-1)\times n}$.

The optimization problem for stimulation pulses with adjustable amplitude is described by the expression

$$\begin{aligned} &\min_{\vec{x}} \ \|a_s T_e \vec{x} + B_s - \vec{y}_{\text{ref}}\|_2 \\ &\text{subject to} \\ &x[k] \in [-1, 0], \, k = 0, \ldots, n-1. \end{aligned} \quad (12)$$

In the above optimization problem, a_s is set equal to the maximum allowed stimulation current. This optimization problem is convex. Therefore, if a solution exists, it is unique and the global minimum [20]. We denote the solution to this optimization problem as $\vec{x}^*$.

For stimulation pulses with binary amplitude values, the optimization problem is

$$\begin{aligned} &\min_{\vec{x}, a_s} \ \|a_s T_e \vec{x} + B_s - \vec{y}_{\text{ref}}\|_2 \\ &\text{subject to} \\ &x[k] \in \{-1, 0\}, \, k = 0, \ldots, n-1 \\ &a_s \in [0, \overline{A}]. \end{aligned} \quad (13)$$

In this case, the constant scalar a_s becomes an optimization variable. $\overline{A}$ is the maximum value that a_s is allowed to take (i.e. maximum stimulation current). The optimal values for this optimization problem are denoted as $\vec{x}^*$ and a_s^*. This optimization problem is not convex. Therefore, a minimum solution, if it exists, is not guaranteed to be unique or global [20]. We used mixed-integer optimization algorithms to compute solutions to the optimization problem (13).

2.3.1. Optimization algorithms and implementation

All the simulations and optimization algorithms were implemented in Matlab (MathWorks, Natick, MA, USA) and a computer equipped with an Intel Core i7-8700 K CPU processor (3.7 GHz) and a 32 GB RAM memory. For the optimization, we integrated the CVX package with Matlab [20] and solutions were

obtained using the Gurobi solver. This solver was chosen because it has the capability of solving both convex and mixed-integer optimization problems [21, 22].

The optimization routines applied to both the low-order and patient-specific models were implemented with 2 s long LFP time series ($n = 360$ samples). This period was sufficient to determine the steady-state stimulation patterns needed to modulate the targeted oscillations. It also enabled us to attain a solution to the mixed-integer optimization problem with a desired gap and within a reasonable time (< 20 s). At each step, the solver internally calculates the best known objective function value for a feasible solution and the objective function lower bound. The optimal objective value is always between these two values. When the relative gap between these objective bounds is smaller than the 'MIPGap' parameter of the solver, the optimization terminates. The MIPGap was set to 0.1 for our optimization.

2.4. Assessment of neural modulation

We quantified the degree of modulation achieved by pulse sequences with adjustable or binary stimulation amplitudes using the optimal value of the optimization cost function $J = \|a_s T_e \vec{x} + B_s - \vec{y}_{ref}\|_2$.

3. Results

3.1. Phase modulation of stimulation pulses mediate optimal suppression and amplification of oscillations with a constant amplitude envelope

The stimulation sequences derived with the nominal generalized model (nominal damping and natural frequency) that optimally suppressed or amplified spontaneous oscillations with constant amplitude consist of pulse trains locked to a specific phase of the oscillations. Figure 4 shows the wavelet scalograms (time–frequency maps) of the modulated signal and the temporal evolution of the targeted oscillations, modulated signal, and stimulation pulses for the following scenarios: suppression of targeted oscillations using pulses with an adjustable amplitude (max. amplitude $a_s = 2.5$ mA), suppression of targeted oscillations using pulses with an adjustable amplitude (max. amplitude $a_s = 0.4$ mA), suppression of targeted oscillations using pulses with the binary amplitude constraint, and amplification of targeted oscillations using pulses with an adjustable amplitude (max. amplitude $a_s = 2.5$ mA). For brevity, we do not show the patterns for pulses with the binary amplitude constraint when amplification was the optimization goal.

The phase locking pattern was observed for pulses with both an adjustable amplitude (figures 4(a)–(d)) and the binary amplitude constraint (figures 4(e) and (f)) when the optimization goal was either suppression or amplification of the targeted oscillations. Nonetheless, the optimal cost for stimulation sequences with an adjustable amplitude ($J = 23.4$ for suppression and $J = 49.3571$ for amplification with $a_s = 2.5$ mA) is smaller than the cost for sequences with the binary amplitude constraint ($J = 410.2$ for suppression and $J = 687.986$ for amplification). The values of J can be compared between pulse types (adjustable vs. constant amplitude) when the same objective (e.g. suppression) is considered. One should not compare values of J in the amplification vs. suppression objectives because the reference vector $\vec{y}_{ref}$ is different in these two scenarios.

We considered two constraints on the maximum stimulation amplitude ($a_s = 2.5$ mA and $a_s = 0.4$ mA) for the pulses with an adjustable amplitude. The relative effect of using a maximum current $a_s = 2.5$ mA vs. $a_s = 0.4$ mA helped us to understand how a decrease in the maximum allowed stimulation amplitude impacts the optimal pulse patterns. Constraints on the stimulation amplitude may be needed when the maximum electrical current cannot exceed a threshold in order to keep the electric charge within safe limits or when side effects due to stimulation need to be avoided. For targeted oscillations with a constant amplitude envelope, a decrease in the maximum allowed stimulation results in an increase in the number of pulses in each train aligned with the phase of the oscillations. See scalograms and pulse patterns in figures 4(a)–(b) vs. (c)–(d). The greater number of pulses in each train results in an increase in the amplitude of the evoked responses (temporal summation) and thereby an enhanced ability to create constructive or destructive interference. It is worth mentioning here that the pulse frequency is limited by the sampling rate used in the mathematical models (i.e. 180 Hz).

3.2. Pulse frequency, amplitude, and phase modulation mediate optimal suppression and amplification of oscillations with a time-varying amplitude envelope

The stimulation sequences that optimally suppress or amplify oscillations with a time-varying amplitude envelope exhibit a combination of phase, frequency, and amplitude pulse modulation for the case in which the pulse's normalized amplitude is allowed to take any value in a continuous range between 0 and 1 (maximum current $a_s = 2.5$ mA). Pulse sequences with a higher frequency and amplitude are generated at specific phases of the spontaneous oscillations to increase the amplitude of the evoked responses and thereby achieve optimal destructive or constructive interference between the spontaneous and evoked oscillations (figures 5(a) and (b)).

For the pulses with an adjustable amplitude, our results indicate that pulse frequency modulation

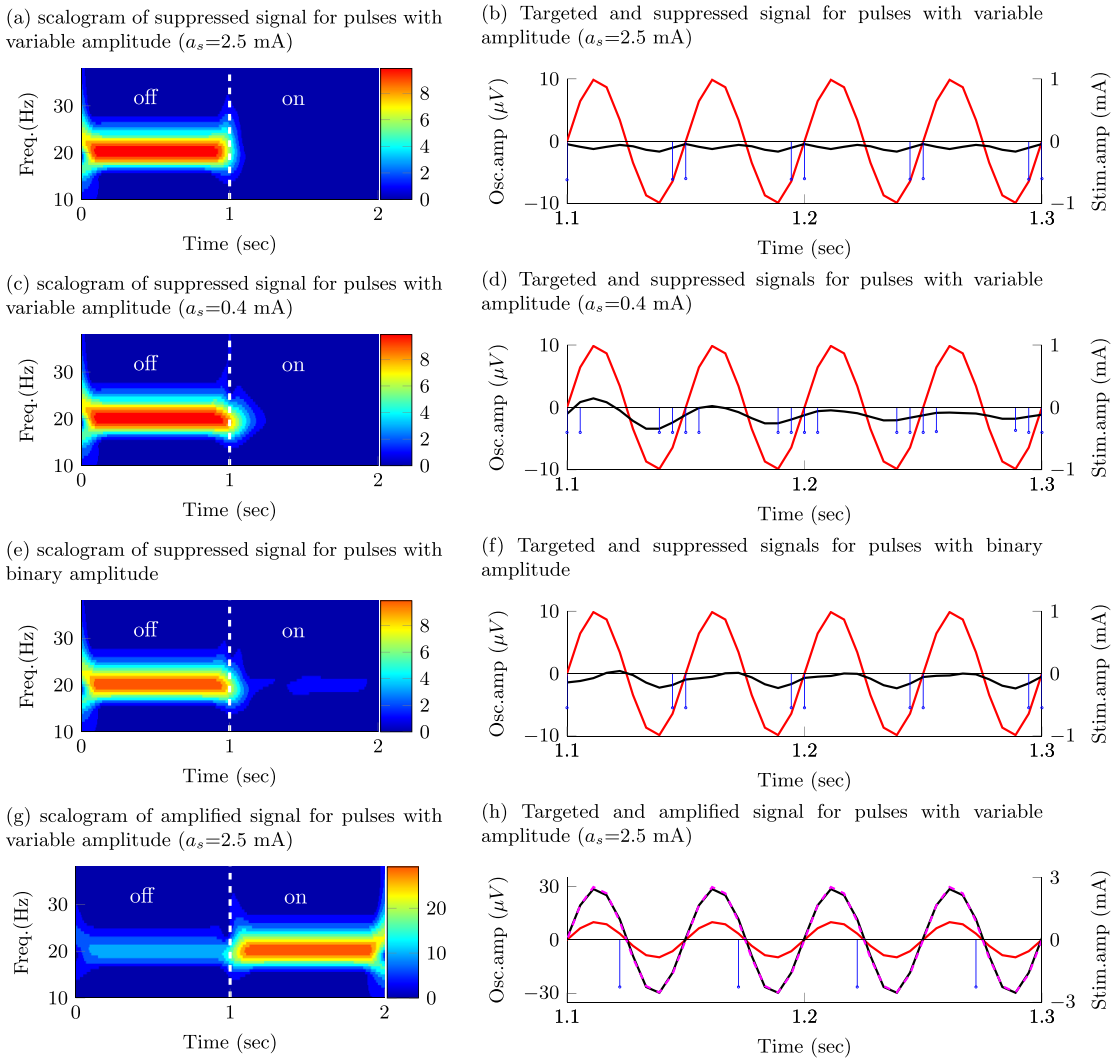

Figure 4. Effect of stimulation pulses on oscillations with constant amplitude envelope. Targeted oscillations (−), modulated (suppressed/amplified) oscillations (−), reference signal for amplification (- -), optimal stimulation sequence (–) Targeted signal, modulated signal, and Wavelet scalograms of the modulated signal during a transition from off- to on-stimulation are shown for sequences with the following characteristics: (a), (b) pulses of adjustable amplitude (max. amplitude $a_s = 2.5$ mA) that suppress the targeted oscillations; (c), (d) pulses of adjustable amplitude (max. amplitude $a_s = 0.4$ mA) that suppress the targeted oscillations; (e), (f) pulses with the binary amplitude constraint that suppress the targeted oscillations; (g), (h) pulses of adjustable amplitude (max. amplitude $a_s = 2.5$ mA) that amplify the targeted oscillations.

becomes more predominant than pulse amplitude modulation to maximize the suppression or amplification of the targeted oscillations as the value of the maximum allowed pulse amplitude (a_s) is reduced from 2.5 to 0.4 mA (figures 5(c) and (d) vs. (a) and (b)).

The solution to the optimization problem with the binary amplitude constraint on the pulses consists of sequences exhibiting a combination of pulse frequency and pulse phase modulation. When suppression was the optimization objective, these pulses were delivered only when the amplitude envelope of the oscillations was above a threshold. See figures 5(f) vs. (b) at time 2.1 s and after. This threshold-based strategy ensures that oscillations evoked by stimulation pulses with a fixed amplitude do not amplify the spontaneous oscillations when these oscillations are small compared to the evoked responses.

The optimization cost associated with the pulses with adjustable amplitude was smaller than the cost associated with the pulses with the binary amplitude constraint (J = 22.7 vs. 353.8 for suppression and J = 54.2147 vs. 912.569 for amplification). Therefore, pulse sequences with adjustable amplitude can achieve greater suppression or amplification than pulses with a binary amplitude constraint. The optimization results and cost function values for the studied pulse amplitude constraints and generalized model are summarized in table 1.

3.3. Changes in the evoked response natural frequency and damping affect the degree of modulation but not the structure of the pulse sequences

The degree by which the optimized stimulation patterns modulate the targeted oscillations depends

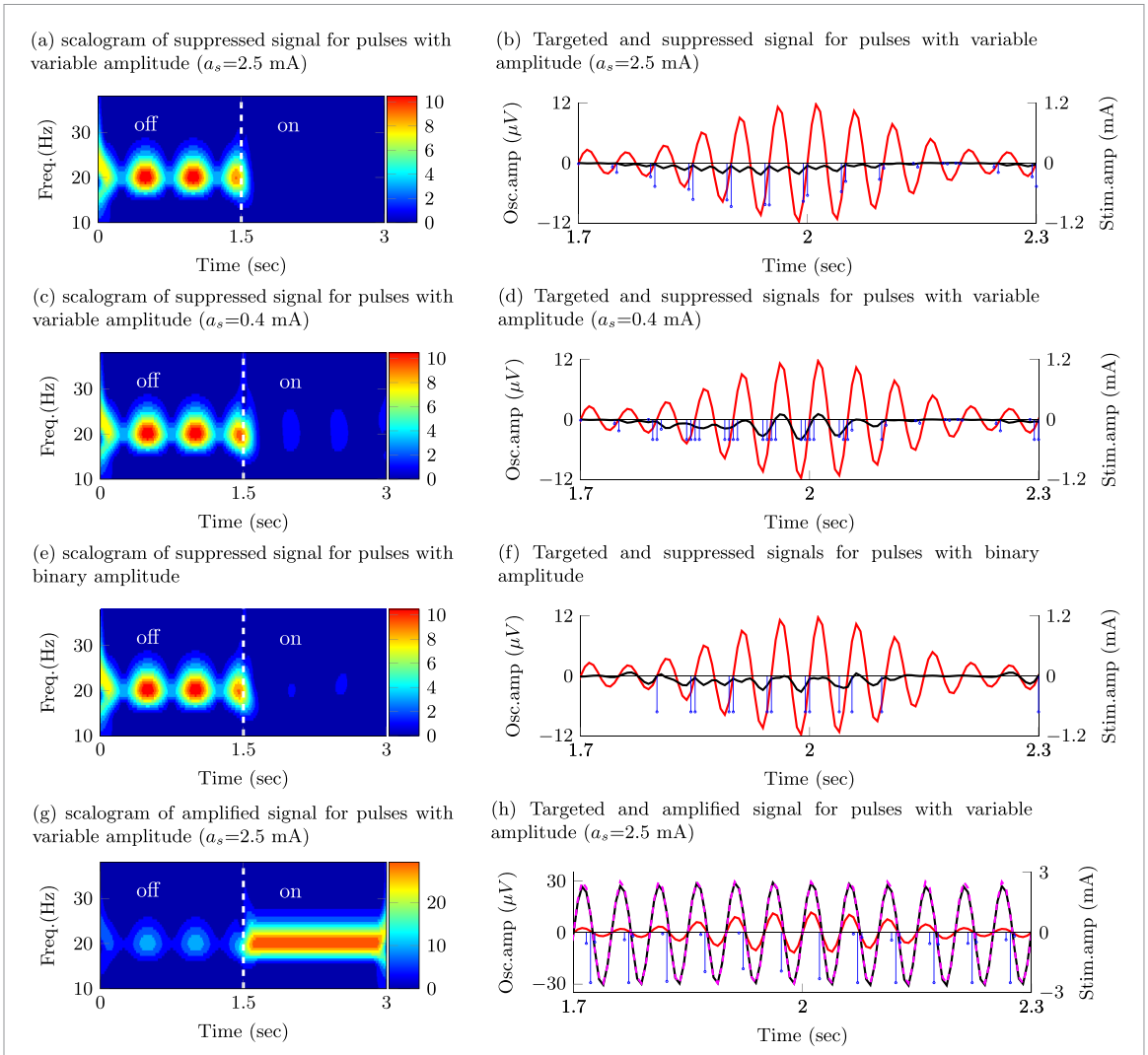

Figure 5. Effect of stimulation pulses on oscillations with time-varying amplitude envelope. Targeted oscillations (—), modulated (suppressed/amplified) oscillations (—), reference signal for amplification (- -), optimal stimulation sequence (—). Targeted signal, modulated signal, and wavelet scalograms of the modulated signal during a transition from off- to on-stimulation are displayed for sequences with the following characteristics: (a), (b) pulses of adjustable amplitude (max. amplitude $a_s - 2.5$ mA) that suppress the targeted oscillations; (c), (d) pulses of adjustable amplitude (max. amplitude $a_s = 0.4$ mA) that suppress the targeted oscillations; (e), (f) pulses of constant amplitude that suppress the targeted oscillations; (g), (h) pulses of adjustable amplitude (max. amplitude $a_s = 2.5$ mA) that amplify the targeted oscillations.

Table 1. Summary of optimization results for the nominal generalized neural dynamics model.

	Oscillations with a constant amplitude envelope	Oscillations with a time-varying amplitude envelope
Stimulation pulses with an adjustable amplitude (max. a_s = 2.5 mA)	Frequency, phase, and amplitude modulation (J = 23.4 for suppression and J = 49.35 for amplification)	Frequency, phase, and amplitude modulation (J = 22.7 for suppression and J = 54.2147 for amplification)
Stimulation pulses with binary amplitude values (max. a_s = 2.5 mA)	Phase modulation (J = 410.2 for suppression and J = 687.986 for amplification)	Phase modulation (J = 353.8 for suppression and J = 912.569 for amplification)

on the damping and natural frequency of the stimulation-evoked responses. The optimization cost is a monotonically increasing function of the damping ratio. Figures 6(b) and (e) show the optimization cost (J) as a function of the damping ratio (ζ) for targeted oscillations with constant and time-varying envelope, respectively. When the natural frequency of the evoked response matches the frequency of the targeted oscillations, the lowest value of the optimization cost function is attained. The optimization cost increases as the natural frequency moves away from the targeted oscillations' frequency. Figures 6(c) and

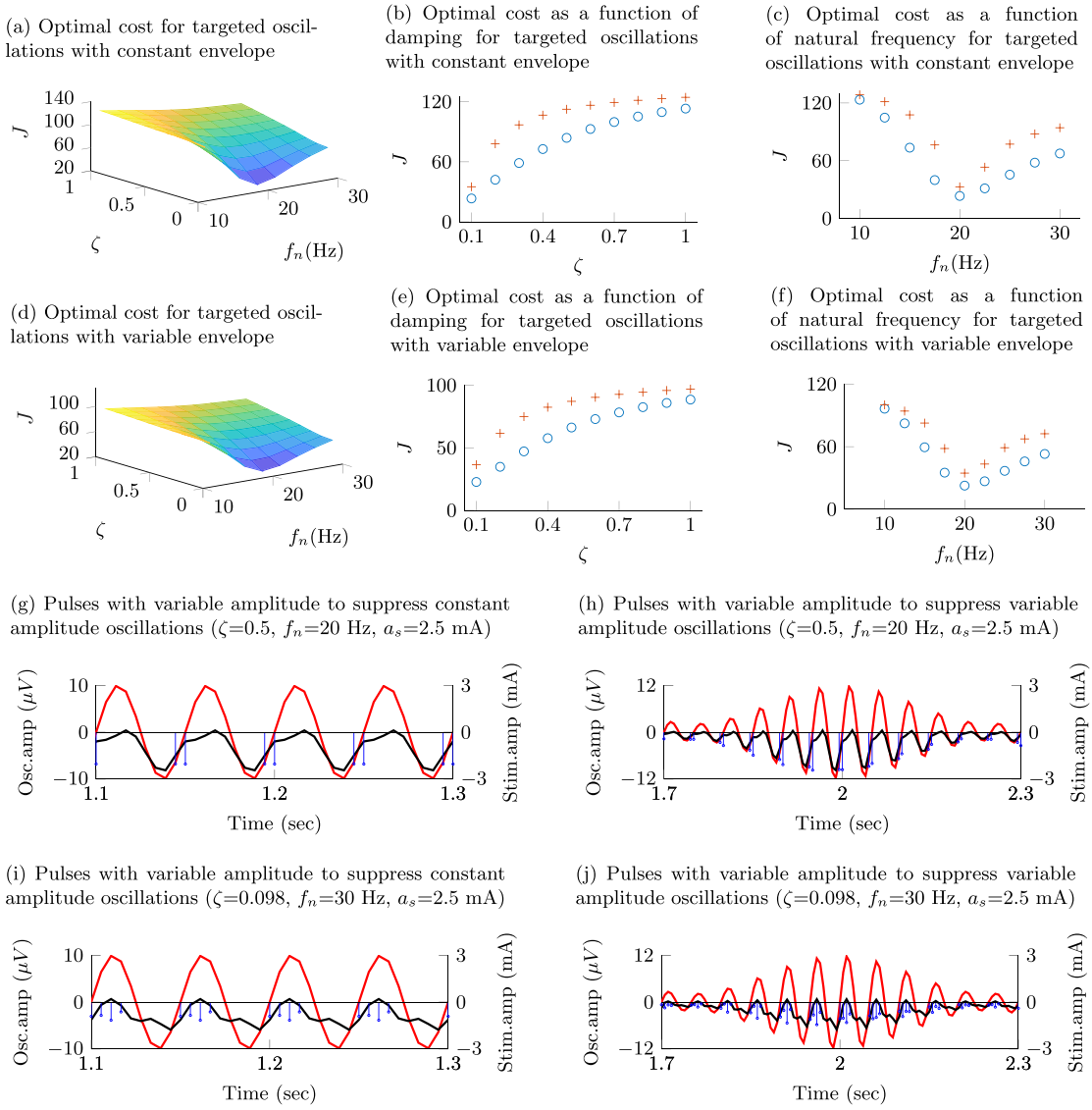

Figure 6. The surface plots in (a) and (d) illustrate the optimal cost function value (J) as a function of the damping ratio (ζ) and natural frequency (f_n) when the targeted oscillations are suppressed via pulse sequences with adjustable amplitude ($a_s = 2.5$ mA). Targeted oscillations with a constant envelope are considered in (a), and with a time-varying envelope in (d). The curves in (b) and (e) show the optimal value of J as a function of ζ when $f_n = 20$ Hz (nominal value) for targeted oscillations with a constant and time-varying envelope, respectively. These curves illustrate the optimal cost function values for pulse sequences with adjustable amplitude whose maximum allowed amplitude (a_s) was set equal to 2.5 mA (∘), and 0.4 mA (+). The curves in (c) and (g) show the optimal value of J as a function of f_n when $\zeta = 0.092$ (nominal value) for targeted oscillations with a constant and time-varying envelope, respectively. Examples of pulse sequences and modulated signals for evoked responses with a damping ratio $\zeta = 0.5$ (different from its nominal value) and $f_n = 20$ Hz (nominal) are shown in (g) and (h) for targeted oscillations with a constant and time-varying envelope, respectively. The plots in (i) and (j) show examples of pulse sequences and modulated signals for evoked responses with $\zeta = 0.092$ (nominal) and $f_n = 30$ Hz (different from nominal) when the targeted oscillations have a constant and time-varying amplitude envelope, respectively.

(f) show the optimization cost (J) as a function of the natural frequency (f_n) for targeted oscillations with a constant and time-varying envelope, respectively.

The structure of the pulse patterns (i.e. pulse phase, amplitude, and frequency modulation) did not change when the damping or natural frequency were varied. Figures 6(g) and (h) illustrate examples of optimal pulse sequences with adjustable amplitude for evoked responses with a damping ratio equal to 0.5 and natural frequency equal to 20 Hz. While this damping ratio significantly departs from the nominal value (0.092), pulse phase modulation is preserved to suppress the targeted oscillations with constant amplitude, and a combination of phase, amplitude, and frequency modulations is preserved to suppress the targeted oscillations with time-varying amplitude. See figures 6(g) vs. 4(b) and 6(h) vs. 5(b). When the nominal natural frequency (20 Hz) is increased to 30 Hz, the pulse phase modulation is preserved to suppress the targeted oscillations with constant

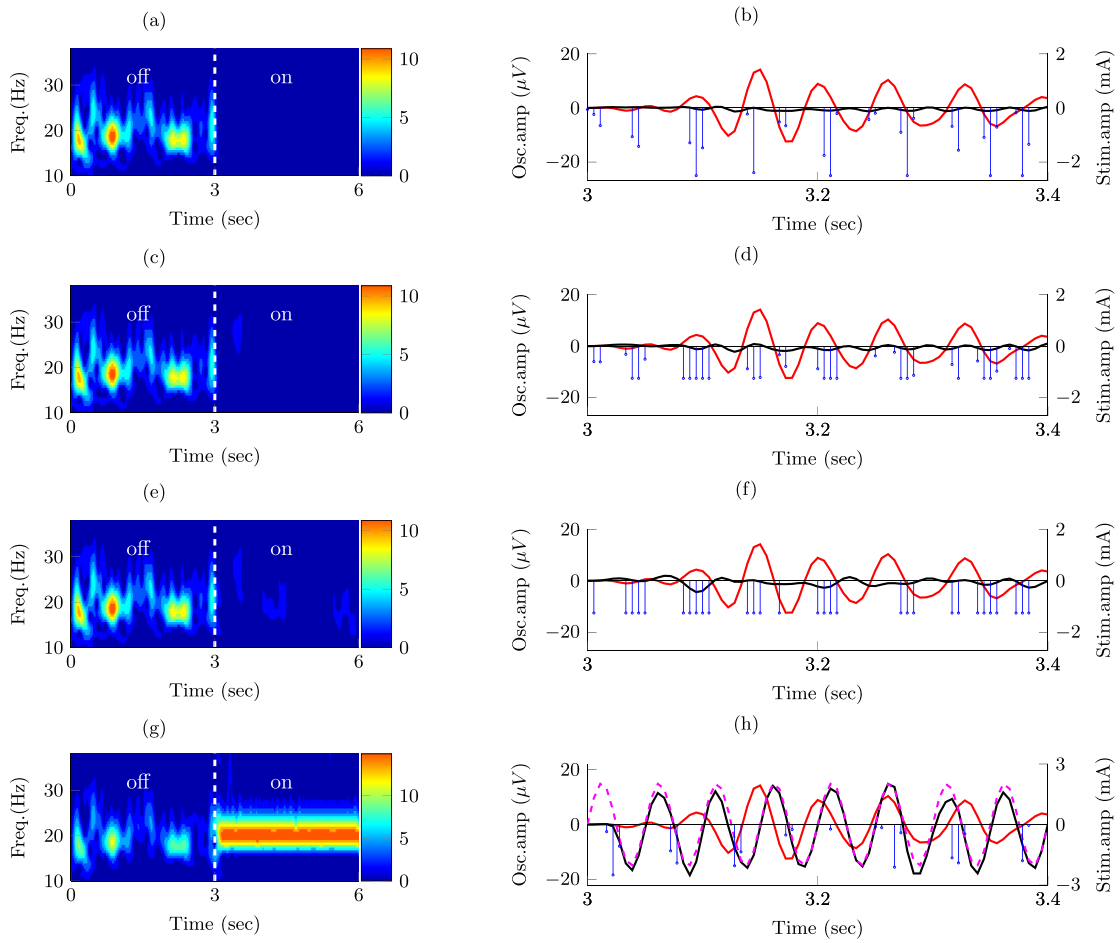

Figure 7. Effect of stimulation pulses on patient-specific GPi neural dynamics. Targeted oscillations (—), modulated (suppressed/amplified) oscillations (—), reference signal for amplification (- -), optimal stimulation sequence (—). Targeted signal, modulated signal, and wavelet scalograms of the modulated signal during a transition from off- to on-stimulation for sequences with the following characteristics: (a), (b) pulses of adjustable amplitude (max. amplitude $a_s - 2.5$ mA) that suppress the targeted oscillations; (c), (d) pulses of adjustable amplitude (max. amplitude $a_s = 1.25$ mA) that suppress the targeted oscillations; (e), (f) pulses of constant amplitude that suppress the targeted oscillations; (g), (h) pulses of adjustable amplitude (max. amplitude $a_s = 2.5$ mA) that amplify the targeted oscillations.

amplitude, and the combination of phase, amplitude, and frequency modulations is preserved to suppress the targeted oscillations with time-varying amplitude. See figures 6(i) vs. 4(b) and 6(j) vs. 5(b).

3.4. Stimulation sequences for patient-specific neural dynamics model matched those obtained with the generalized model

Stimulation pulse sequences with adjustable amplitude employed frequency, phase, and amplitude pulse modulation to attain maximum suppression or amplification of targeted oscillations in the patient-specific model of the GPi neural dynamics (figures 7(a) and (b)). As we reduced the maximum allowed stimulation amplitude from 2.5 mA to 1.25 mA, frequency modulation rather than amplitude modulation dominated the pulse patterns to achieve maximum suppression (figures 7(c) and (d)). Stimulation pulses with the binary amplitude constraint used phase and frequency modulation to modulate the targeted oscillations (figures 7(e) and (f)). The reduction in the 2-norm of the modulated signal was greater for the adjustable amplitude pulses ($J = 23.4$ for suppression and $J = 49.3571$ for amplification) than for the binary amplitude pulses ($J = 410.2$ for suppression and $J = 687.986$ for amplification). These results agree with those obtained with the generalized neural dynamics model.

Figure 8 shows the PSD curves of the modulated signal when the optimization goal was to suppress or amplify the targeted neural activity. These PSD curves show that stimulation pulses with both adjustable and binary amplitudes can effectively modulate the mean power of frequency specific neural oscillations in the targeted frequency band (14–24 Hz). They also indicate that the mean power reduction attained via pulses with adjustable amplitude is comparable to the reduction achieved via pulses with the binary amplitude constraint, even though the difference in the cost function values was more notable.

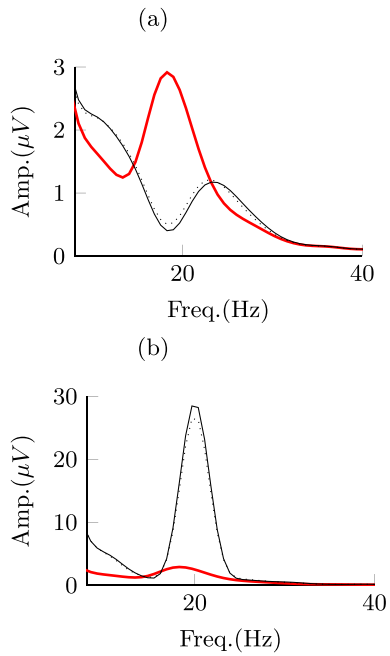

Figure 8. Power spectral density (PSD) curves of neural activity in the internal segment of the globus pallidus from a patient-specific mathematical model. PSD curves shown in the figure are associated with periods in the off-stimulation condition (—) and when stimulation pulses with adjustable amplitude (—) and the binary amplitude constraint (····) were delivered. (a) and (b) show PSD curves during periods of suppression and amplification of frequency-specific neural activity, respectively.

4. Discussion

In this study, we identified electrical pulse patterns to effectively modulate spontaneous neural oscillations using stimulation-evoked neural responses. We leveraged mathematical optimization tools to discover pulse patterns that minimize (or maximize via reference tracking) the 2-norm of frequency-specific neural oscillations. To identify these pulse patterns, we employed neurophysiologically-inspired mathematical models of spontaneous and stimulation-evoked oscillations. We considered stimulation-evoked response models with distinct natural frequency and damping coefficient as well as a subject-specific GPi model of a Parkinson's disease patient. The distinct neural dynamics studied here enabled us to assess whether optimized pulse sequences preserve their structure. Our analysis revealed that, across the studied neural dynamics, a combination of phase, amplitude, and frequency modulation of the electrical pulses results in optimal suppression or amplification of the targeted oscillations. These pulse modulation strategies provide the rationale for the development of future closed-loop neuromodulation systems that employ stimulation-evoked responses and pulse modulation strategies to effectively control neural activity in real-time. These closed-loop neurostimulation systems could, in turn, be key to characterize the role of neural activity in brain function and ultimately advance personalized neuromodulations therapies.

4.1. Mechanisms underlying optimized neural modulation

The optimized stimulation sequences identified in this study take advantage of phase, frequency and amplitude pulse modulation to achieve optimal suppression or amplification of targeted oscillations. Phase modulation (or time alignment) of the pulse trains relative to the targeted oscillations' phase is required to effectively achieve either destructive or constructive interference between the spontaneous and evoked oscillations. We showed that when the amplitude envelope of the spontaneous oscillations is constant over time, phase modulation (or locking) is sufficient to achieve optimal suppression or amplification of the targeted oscillations. However, the envelope of real *in-vivo* spontaneous oscillations is not constant over time [12, 14]. Our results show that adjustments in the stimulation pulse frequency and amplitude are needed to create precise destructive or constructive interference between stimulation-evoked responses and spontaneous oscillations whose amplitude envelope varies over time. Pulse frequency modulation results in changes in the evoked response amplitude because of the principle of superposition (or temporal summation) observed in responses to stimulation trains [23–25]. For this superposition or temporal summation to be effective, the intra-burst period of the pulse trains must be greater than the refractory period of the neuronal population being stimulated with the electrical pulses. If the inter-pulse period is smaller than the refractory period of the neural circuitry being activated, a temporal summation of evoked responses is not expected to occur [24, 26, 27]. Pulse amplitude modulation can be employed, in addition or instead of frequency modulation, to adjust the evoked responses' amplitude and suppress the spontaneous oscillations. Because the pulse amplitude (voltage or current) is limited in FDA-cleared or -approved neurostimulation devices to minimize the likelihood of tissue damage, we studied the effect of constraining the pulse amplitude on the pulse patterns. Our results indicate that when the maximum allowed pulse amplitude (upper bound) is reduced, frequency pulse modulation becomes more predominant than amplitude pulse modulation in order to achieve optimal suppression or amplification of the targeted oscillations. This trade-off is important for the implementation of closed-loop neuromodulation systems since they can use a combination of amplitude and frequency pulse

modulation to attain a desired modulation performance given the device constraints and safety envelope.

4.2. Generalization of results

We employed a generalized, low-order mathematical model of stimulation-evoked neural dynamics to characterize optimal pulse sequences that suppress (or amplify) spontaneous neural oscillations. The low-order model was characterized by a single natural frequency and damping coefficient. We studied the effect of varying these two parameters on the optimized pulse sequences to understand how invariant are the pulse modulation strategies across distinct neural dynamics. We also used a model of spontaneous and stimulation-evoked neural activity in the GPi of a Parkinson's disease patient to identify the optimal pulse sequences in a more realistic scenario. Our results indicate that the structure of the optimal pulse patterns (phase, amplitude, and frequency pulse modulation) did not change when the stimulation-evoked neural dynamics were varied or when using the patient-specific model. This consistency across models indicates that pulse modulation strategies can be applied to suppress or amplify neural activity in distinct brain circuits and conditions, whenever spontaneous and stimulation-evoked responses of comparable magnitude are generated in the targeted neuronal population. For example, underdamped neural responses in the hippocampus CA1 area evoked by stimulation of the endopiriform nucleus [28] could be employed, together with our pulse modulation strategies, to control hippocampal, frequency-specific neural activity.

4.3. From optimal pulse sequences to real-time closed-loop neuromodulation

How to embed the optimal pulse sequences studied in this article onto closed-loop stimulation devices is yet to be investigated. A foreseeable approach is to take the pulse sequences from a subject-specific model and embed them onto a closed-loop control system that adjusts the phase, amplitude, and frequency of the pulses based on real-time measurements of the oscillations' amplitude and phase. A major challenge to implement this approach is that pulse sequences calculated using the proposed optimization are obtained based on knowledge of all the spontaneous oscillations samples (from $k = 0$ to $k = n$). Therefore, pulses delivered at time k depend on future values ($k+1, k+2, \ldots$) of the spontaneous oscillations. This strategy is not possible to implement in a real-time system unless a prediction of future neural activity is available. Delivering the optimized pulse sequences based on present and past values of the modulated neural activity (i.e. delayed version of the optimal pulse sequence) may provide greater neuromodulation performance than phase-locked stimulation alone, but likely a reduced performance compared to the optimal stimulation sequences identified in this study because of the time delay introduced in the feedback loop. Future studies need to assess the performance of closed-loop systems with phase, amplitude, and frequency pulse modulation in order to optimize neural control technology. These technology advancements will be key to characterize how controlled changes in neural activity relate to brain function in the healthy and disease states, and to develop therapies tailored to each patient.

4.4. Limitations

To characterize the optimal pulse modulation sequences, we used models of the stimulation evoked responses that consist of a linear dynamical system with stimulation inputs constrained to be square pulses. This model does not consider limits in the amplitude of the evoked and spontaneous neural oscillations and other nonlinearities present in neural circuits. Not including the nonlinear dynamics into the mathematical models can lead to inaccuracies in the pulse sequences calculated via the optimization routines. Nevertheless, our results are valid when considering neural dynamics operating in the linear region. Additionally, introducing a nonlinear element into the mathematical model of the evoked and spontaneous oscillations can result in a non-convex optimization problem whose solution is not guaranteed to be global.

This study is also limited to stimulation sequences optimal when measuring the 2-norm of the targeted oscillations. We selected the 2-norm because it enables us to formulate a convex optimization problem and is intuitive mathematically. Yet, other norms (e.g. 1-norm and ∞-norm) and other cost functions may be more relevant for particular problems in neuroscience and to test specific hypotheses. For example, one may want to use the ∞-norm to determine the pulse sequences needed to minimize the peak amplitude that oscillations can attain.

Data availability statement

All data that support the findings of this study are included within the article (and any supplementary files).

Acknowledgments

Research reported in this publication was funded by the National Institute of Neurological Disorders and Stroke (R01-NS129600 P50-NS123109, R01-NS037019, R37-NS077657), the Wallin Discovery Fund, the Engdahl Family Foundation, and the University of Minnesota's MnDRIVE (Minnesota's Discovery, Research and Innovation Economy)

Initiative-Postdoctoral Neuromodulation Fellowship granted to Hafsa Farooqi.

Author contributions

Hafsa Farooqi: Methodology, Software, Validation, Visualization, Writing—Original Draft. Jerrold L Vitek: Resources, Writing—Review and Editing, Funding Acquisition. David Escobar Sanabria: Conceptualization, Methodology, Software, Validation, Resources, Writing—Original Draft, Writing—Review and Editing, Supervision, Project Administration, Funding Acquisition.

ORCID iD

David Escobar Sanabria https://orcid.org/0000-0001-6402-806X

References

[1] Hanrahan S J, Nedrud J J, Davidson B S, Farris S, Giroux M, Haug A, Mahoor M H, Silverman A K, Zhang J J and Hebb A O 2016 Long-term task- and dopamine-dependent dynamics of subthalamic local field potentials in Parkinson's disease *Brain Sci.* **6** 57

[2] Staub F, Neumann W-J, Horn A, Schanda J, Schneider G-H, Brown P and Kühn A 2016 EP 4. long term recordings of deep brain activity from the subthalamic nucleus in PD patients using PC+S *Clin. Neurophysiol.* **127** e176

[3] Buzsáki G, Anastassiou C A and Koch C 2012 The origin of extracellular fields and currents — EEG, ECoG, LFP and spikes *Nat. Rev. Neurosci.* **13** 407–20

[4] Herreras O 2016 Local field potentials: myths and misunderstandings *Front. Neural Circuits* **10** 101

[5] Brown P 2003 Oscillatory nature of human basal ganglia activity: relationship to the pathophysiology of Parkinson's disease *Mov. Disorders* **18** 357–63

[6] Brown P and Williams D 2005 Basal ganglia local field potential activity: character and functional significance in the human *Clin. Neurophysiol.* **116** 2510–9

[7] Brown P, Oliviero A, Mazzone P, Insola A, Tonali P and Di Lazzaro V 2001 Dopamine dependency of oscillations between Subthalamic nucleus and pallidum in Parkinson's disease *J. Neurosci.* **21** 1033–8

[8] Kühn A A, Kupsch A, Schneider G-H and Brown P 2006 Reduction in subthalamic 8–35 Hz oscillatory activity correlates with clinical improvement in Parkinson's disease *Eur. J. Neurosci.* **23** 1956–60

[9] Kühn A A, Tsui A, Aziz T, Ray N, Brücke C, Kupsch A, Schneider G-H and Brown P 2009 Pathological synchronisation in the subthalamic nucleus of patients with Parkinson's disease relates to both bradykinesia and rigidity *Exp. Neurol.* **215** 380–7

[10] Little S, Pogosyan A, Kuhn A and Brown P 2012 Beta band stability over time correlates with Parkinsonian rigidity and bradykinesia *Exp. Neurol.* **236** 383–8

[11] Blumenfeld Z and Brontë-Stewart H 2015 High frequency deep brain stimulation and neural rhythms in Parkinson's disease *Neuropsychol. Rev.* **25** 384–97

[12] Escobar Sanabria D, Johnson L A, Yu Y, Busby Z, Nebeck S, Zhang J, Harel N, Johnson M D, Molnar G F and Vitek J L 2020 Real-time suppression and amplification of frequency-specific neural activity using stimulation evoked oscillations *Brain Stimul.* **13** 1732–42

[13] McNamara C G, Rothwell M and Sharott A 2022 Stable, interactive modulation of neuronal oscillations produced through brain-machine equilibrium *Cell Rep.* **41** 111616

[14] Escobar Sanabria D *et al* 2022 Controlling pallidal oscillations in real-time in Parkinson's disease using evoked interference deep brain stimulation (eiDBS): proof of concept in the human *Brain Stimul.* **15** 1111–9

[15] Deco G, Jirsa V K, Robinson P A, Breakspear M, Friston K and Sporns O 2008 The dynamic brain: from spiking neurons to neural masses and cortical fields *PLoS Comput. Biol.* **4** 1–35

[16] Bay J 1999 Fundamentals of linear state space systems

[17] Ogata K 2010 *Modern Control Engineering* (*Instrumentation and Controls Series*) (Prentice Hall)

[18] U.S. food and drug administration (www.accessdata.fda.gov/cdrh_docs/pdf14/P140009S039B.pdf) (Accessed 13 February 2022)

[19] Diamond S and Boyd S 2015 Convex optimization with abstract linear operators *Proc. IEEE Int. Conf. on Computer Vision* pp 675–83

[20] Boyd S, Boyd S P and Vandenberghe L 2004 *Convex Optimization* (Cambridge University Press)

[21] Anand R, Aggarwal D and Kumar V 2017 A comparative analysis of optimization solvers *J. Stat. Manage. Syst.* **20** 623–35

[22] Jablonský J *et al* 2015 Benchmarks for current linear and mixed integer optimization solvers *Acta Univ. Agric. Silvic. Mendel. Brunen.* **63** 1923–8

[23] Escobar Sanabria D, Johnson L A, Nebeck S D, Zhang J, Johnson M D, Baker K B, Molnar G F and Vitek J L 2017 Parkinsonism and vigilance: alteration in neural oscillatory activity and phase-amplitude coupling in the basal ganglia and motor cortex *J. Neurophysiol.* **118** 2654–69

[24] Awad M Z, Vaden R J, Irwin Z T, Gonzalez C L, Black S, Nakhmani A, Jaeger B C, Bentley J N, Guthrie B L and Walker H C 2021 Subcortical short-term plasticity elicited by deep brain stimulation *Ann. Clin. Transl. Neurol.* **8** 1010–23

[25] Yeomans J S, Rosen J B, Barbeau J and Davis M 1989 Double-pulse stimulation of startle-like responses in rats: refractory periods and temporal summation *Brain Res.* **486** 147–58

[26] Fehlings M G, Tator C H, Linden R D and Piper I R 1988 Motor and somatosensory evoked potentials recorded from the rat *Electroencephalogr. Clin. Neurophysiol.* **69** 65–78

[27] Bishop P, Jeremy D and Lance J 1953 Properties of pyramidal tract *J. Neurophysiol.* **16** 537–50

[28] Li D *et al* 2020 Electrical stimulation of the endopiriform nucleus attenuates epilepsy in rats by network modulation *Ann. Clin. Transl. Neurol.* **7** 2356–69